Mixture Theory Model Sensitivity to Effective Viscosity in Simulations of Sandy Bedform Dynamics

Allison M. Penko*†, Joseph Calantoni‡ and Donald N. Slinn§
* Naval Research Laboratory, Stennis Space Center, MS 39529, allison.penko@nrlssc.navy.mil, (228) 688–4823
† University of Florida, Dept. of Civil and Coastal Engineering, Gainesville, FL 32607
‡ Naval Research Laboratory, Stennis Space Center, MS 39529, joe.calantoni@nrlssc.navy.mil, (228) 688–4435
§University of Florida, Dept. of Civil and Coastal Engineering, Gainesville, FL 32607, slinn@coastal.ufl.edu, (352) 392–9537

***Abstract*— We perform a sensitivity analysis on a three-dimensional bottom boundary layer model (SedMix3D) that uses mixture theory to simulate the flow and sediment transport over rippled sand beds. SedMix3D treats the fluid-sediment mixture as a single continuum with effective properties that parameterize the fluid-sediment and sediment-sediment interactions using several closures for the sediment phase. The effective viscosity is one such closure that includes three adjustable parameters: the intrinsic viscosity, the maximum viscosity, and the maximum packing concentration of unconsolidated sediment. The sensitivity of suspended sediment concentration predictions by SedMix3D is tested by varying the intrinsic viscosity, which is a proxy for sediment grain shape. We qualitatively and quantitatively analyze the model output of suspended sediment concentration for a range of intrinsic viscosity values typical of quartz sand. Intrinsic viscosity values ranging from 2.5 to 3.5 produce total suspended sediment concentrations that differ less than 11%. However, there is approximately a 16% difference between the suspended sediment concentrations from intrinsic viscosity values of 2.5 to 3.5 and 4.0 to 5.0. Simulations of sediment transport over bedforms performed here were not significantly sensitive to the choice of an intrinsic viscosity value in the range of 2.5 to 3.5. Using a baseline intrinsic viscosity value of 3.0, we subsequently tested two additional effective viscosity formulations. The suspended sediment concentrations predicted by the Eilers and Krieger-Dougherty formulations were very similar, but the Mooney formulation generated much less suspended sediment. We found the model to be more sensitive to variations of effective viscosity in the ripple-fluid interface than in the suspension range.**

I. Introduction

The local properties of the seafloor such as bedform size and shape, grain size distribution, and sediment type all influence bottom boundary layer flow, wave energy dissipation, and sediment erosion and deposition in the coastal region. Past research has focused on predicting the turbulent flow over fixed bedforms, ignoring the response of the flow to resulting sediment transport and changes in bed morphology [1]–[3]. A complete understanding of the feedback between the fluid and sediment in a turbulent bottom boundary layer is necessary for accurate prediction of bedform profile changes and migration rates.

We implement a three-dimensional bottom boundary layer model (SedMix3D) using mixture theory to simulate the coupled interaction between the fluid and sediment. SedMix3D treats the fluid-sediment mixture as a single continuum with effective properties that parameterize the fluid-sediment and sediment-sediment interactions using a variable mixture viscosity, a concentration specific settling velocity, and a shear-induced, empirically calibrated, mixture diffusion term. While mixture theory has been well studied for many types of particle laden flows [4]–[9], and yields reasonable comparisons with laboratory experiments, it has not yet been applied to coastal sediment transport.

The closure for the effective viscosity of the mixture is a function dependent on the local sediment concentration, the sediment shape, the maximum viscosity, and the maximum packing concentration. The documented relationships for the effective viscosity have two common features. In dilute suspensions, concentration and viscosity are linearly related [10], and at a certain maximum packing concentration, the viscosity becomes infinite [11]. Studies have found that viscosities modeled by concentration dependent equations compare well with viscosity measurements of small particles ($O(0.001\ \mathrm{cm})$) in suspension [12]–[19] and large particles ($O(0.01\ \mathrm{cm})$) in dense concentrations (up to 0.70 volume fraction) [20], [21]. We use an effective viscosity formulation in the form of an Eilers' equation [11] and choose the maximum packing concentration to be 0.63, roughly equivalent to random close packing for identical spheres. The intrinsic viscosity parameter, $[\mu]$, accounts for the particle shape [22] and has been well documented for spherical particles as 2.5 [10]. For irregularly shaped particles, $[\mu]$ is still largely uncertain [15]. Here, we tested the sensitivity of the sediment phase closure for effective viscosity by varying the intrinsic viscosity and examining changes in suspended sediment concentration. Additionally, we chose a single intrinsic viscosity and compared suspended sediment concentrations for three different effective viscosity formulations.

0-933957-38-1 ©2009 MTS

II. Methodology

A. Governing Equations

The governing equations for SedMix3D include a sediment continuity, mixture continuity, and mixture momentum equations. The sediment phase closures include a mixture viscosity formulation, a shear induced diffusion term, and a hindered settling function. The mixture continuity equation is derived by combining the fluid and sediment phase continuity equations,

$$\frac{\partial \rho}{\partial t} + \nabla \cdot (\rho \mathbf{u}) = 0, \tag{1}$$

where $\mathbf{u}$ is the mixture velocity and ρ is the mixture density,

$$\rho = \phi \rho_s + (1 - \phi)\rho_f, \tag{2}$$

where ϕ is the sediment volume fraction, and ρ_s and ρ_f are the sediment and fluid densities, respectively.

The mixture momentum equation is also derived from the sum of the individual phase momentum equations. The mixture stresses can be defined by assuming the mixture behaves as a Newtonian fluid [23] resulting in,

$$\rho \frac{\partial \mathbf{u}}{\partial t} + \rho \mathbf{u} \cdot \nabla \mathbf{u} = -\nabla P + \nabla \cdot (\mu \nabla \mathbf{u}) + \mathbf{F} - \rho \mathbf{g}, \tag{3}$$

where P is the mixture pressure, μ is the mixture viscosity, $\mathbf{F}$ is the external driving force vector per unit volume, and $\mathbf{g}$ is gravitational acceleration ($981\ \mathrm{cm\ s^{-2}}\ \hat{k}$). SedMix3D employs a modified Eilers equation [11] to represent mixture viscosity, μ, here scaled by the pure water viscosity, μ_f,

$$\frac{\mu}{\mu_f} = \left[1 + \frac{0.5[\mu]\phi}{1 - \phi/\phi_m}\right]^2, \tag{4}$$

where $[\mu]$ is the intrinsic viscosity, a dimensionless parameter representing the sediment grain shape, and $0.0 \leq \phi \leq 0.63$, where the lower bound represents pure water and upper bound roughly corresponds to the maximum concentration of unconsolidated sediment. Here, we fix the maximum value of the mixture viscosity by specifying $\phi_m = 0.644$. The external driving force, $\mathbf{F}$, approximates the horizontal pressure gradient produced by the passage of a surface gravity wave. Here we use a simple sinusoidal forcing in the x-direction with amplitude, U_o and period, T (Figure 1),

$$\mathbf{F} = \rho_f U_o \left(\frac{2\pi}{T}\right) \cos\left(\frac{2\pi}{T} t\right) \hat{i}. \tag{5}$$

The concentration of sediment is modeled with a sediment continuity equation [4] that describes the balance of sediment flux by advection, gravity, and shear-induced diffusion,

$$\frac{\partial \phi}{\partial t} + \mathbf{u} \cdot \nabla \phi = D \nabla^2 \phi - \frac{\partial \phi W_t}{\partial z}, \tag{6}$$

where W_t is the concentration specific settling velocity [24],

$$W_t = W_{t0}(1 - \phi)^q, \tag{7}$$

where W_{t0} is the settling velocity of a single particle in a clear fluid and q is an empirical constant,

$$q = \begin{cases} 4.35 Re_p^{-0.03} & 0.2 < Re_p \leq 1, \\ 4.35 Re_p^{-0.10} & 1 < Re_p \leq 500, \\ 2.39 & 500 < Re_p. \end{cases} \tag{8}$$

Re_p is defined as the particle Reynolds number,

$$Re_p = \frac{d \rho_f |W_{t0}|}{\mu_f} \tag{9}$$

where d is the sediment grain size diameter (0.04 cm). We consider only non-cohesive grains with the material properties of quartz in water ($\rho_s = 2.66$ g/cm^3). The closure for the shear-induced diffusion of sediment, D, is a function of particle size, concentration, and mixture stresses [25]. Assuming isotropic diffusion (i.e., $D_{xx} = D_{yy} = D_{zz}$),

$$D = \frac{1}{4} d^2 \beta(\phi) |\nabla \mathbf{u}|, \tag{10}$$

where $|\nabla \mathbf{u}| \equiv \sqrt{\frac{1}{2}(\mathbf{u} : \mathbf{u}^{\mathbf{T}})}$ and $\beta(\phi)$ is an empirically determined coefficient,

$$\beta(\phi) = \alpha \phi^2 \left(1 + \frac{1}{2} e^{8.8\phi}\right), \tag{11}$$

where α is an empirical constant found to be approximately 0.33 for large values of the Shields parameter ($0.5 < \theta < 30$) by combining results from the dilute limit with measurements in dense concentration suspensions. It is noted that the above formulation may result in an underestimation of the diffusion coefficient [25].

The model uses a finite volume method with a staggered grid to solve the time-dependent sediment concentration function and the mass and momentum conservation equations for the fluid-sediment mixture to second-order accuracy in space and third-order accuracy in time. With grid spacing

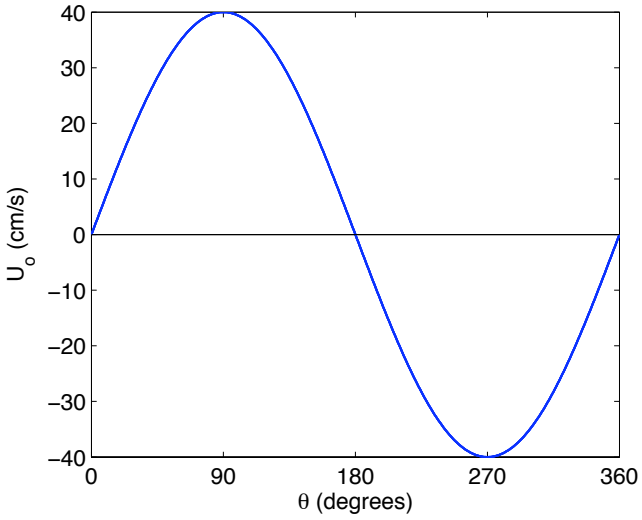

Fig. 1. The free stream velocity time series for a wave period.

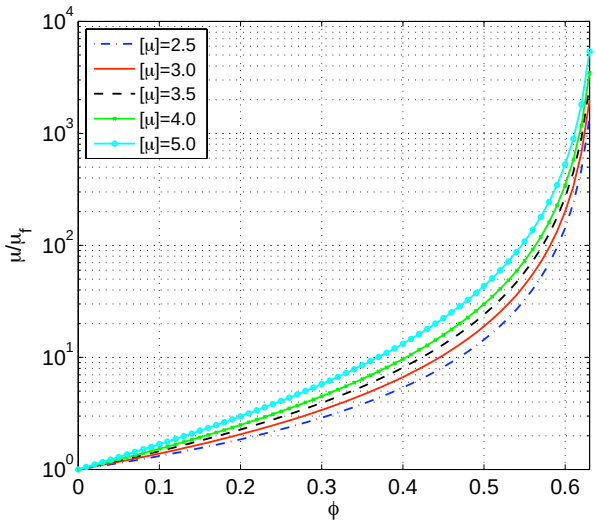

Fig. 2. The scaled effective viscosity (4) resulting from varying intrinsic viscosities, $[\mu]$, versus volume fraction of sediment, ϕ.

typically about an order of magnitude less than the smallest (Kolmogorov) turbulent length scale and time steps nearly four orders of magnitude less than the smallest turbulent temporal scale, we consider SedMix3D to be a direct numerical simulation.

III. Results

A. Intrinsic Viscosity

We tested the model sensitivity to the choice of intrinsic viscosity in (4) by examining the suspended sediment concentration output from five simulations with identical forcing but with varying intrinsic viscosities ranging from $2.5 \leq [\mu] \leq 5.0$, which represent a wide range of possible grain shapes. Figure 2 is a plot of the scaled effective viscosity of the mixture (4) versus volumetric concentration, ϕ, for the varying intrinsic viscosities. The intrinsic viscosity is a function of the particle's axis ratio, r (particle length:particle width) [22]. Mixtures with long, flat particles will have larger intrinsic viscosities than mixtures with sphere-like particles. The intrinsic viscosity of a fluid-sediment mixture with spherical sand particles ($r = 1$) has been documented as 2.5 [10]. We use 2.5 as a base value and compare simulations with intrinsic viscosities of 3.0, 3.5, 4.0, and 5.0. An intrinsic viscosity of 5.0 corresponds to a particle axis ratio of approximately 5:1.

The simulated flow has a maximum free stream velocity of 40 cm/s and a 2 s period (Figure 1). The sediment size was fixed at 0.04 cm. We initialized the simulations with a sinusoidal ripple of height 1 cm and length 12 cm. The simulations ran for 5 wave periods (10 s). Although the model is fully three-dimensional, the simulations ran here contained only two grid points in the y-direction to reduce the computational time necessary to obtain 10 s of real-time output. See the Discussion for an explanation of model grid resolution. We summed the concentration fields in the y-direction and ensemble averaged over the last three wave periods, allowing 2 wave periods of model spin-up, to obtain concentration fields in the x- and z-domain throughout a full flow phase. Here, we qualitatively compared the ensemble averaged concentration fields at flow reversal ($\theta = 0°$), maximum flow acceleration ($\theta = 45°$), and maximum flow deceleration ($\theta = 135°$) for all five simulations (Figures 3, 4, and 5). For the three phases of the flow shown, the suspended sediment plumes were in similar locations along the ripple profile and at similar heights in the water column in all the simulations. In Figure 3, the free stream velocity is zero and the flow is reversing from left to right. As the flow changed direction, sediment was picked up from the left side of the ripple and advected into the water column. For the simulations with intrinsic viscosities of 4.0 and 5.0 (herein referred to as higher intrinsic viscosity simulations), much less sediment was suspended compared to the simulations with intrinsic viscosity values of 2.5 to 3.5 (herein referred to as lower intrinsic viscosity simulations), but was in similar locations along the ripple profile and at similar heights in the water column.

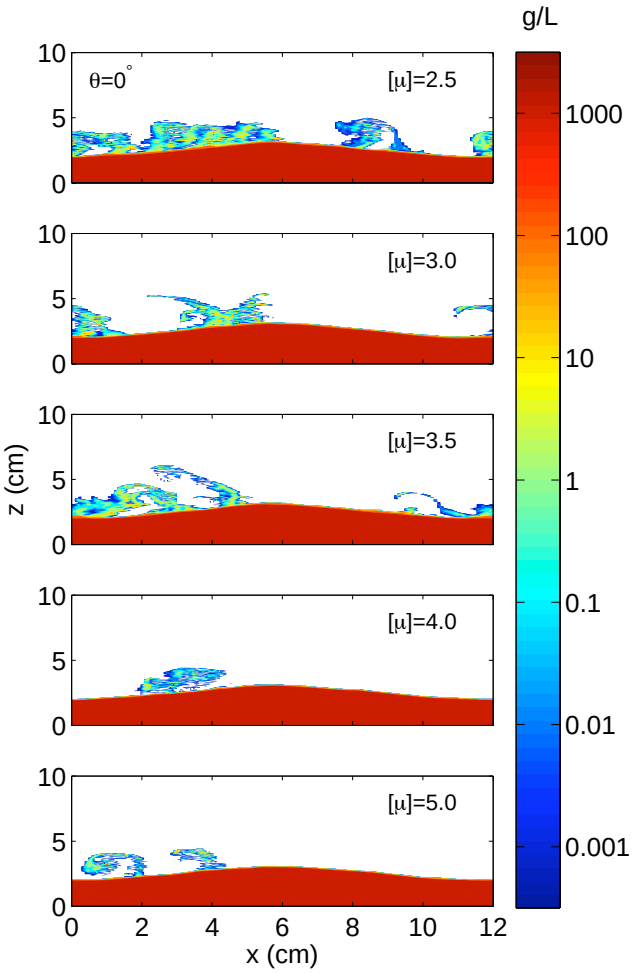

Fig. 3. Suspended sediment concentration fields ensemble averaged over three wave periods at flow reversal ($\theta = 0°$) for varying intrinsic viscosities.

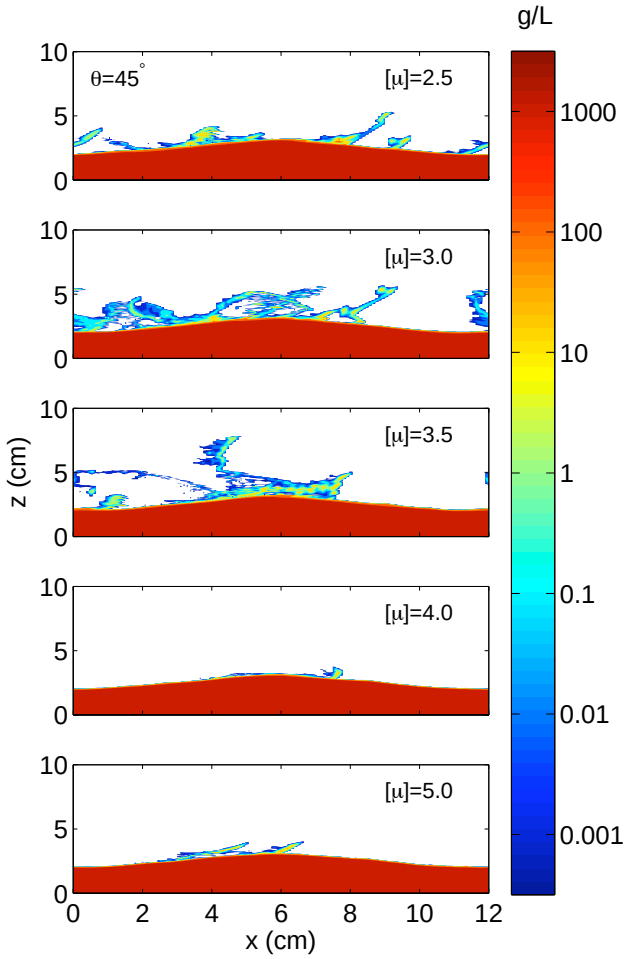

Fig. 4. Suspended sediment concentration fields ensemble averaged over three wave periods at maximum flow acceleration ($\theta = 45°$) for varying intrinsic viscosities.

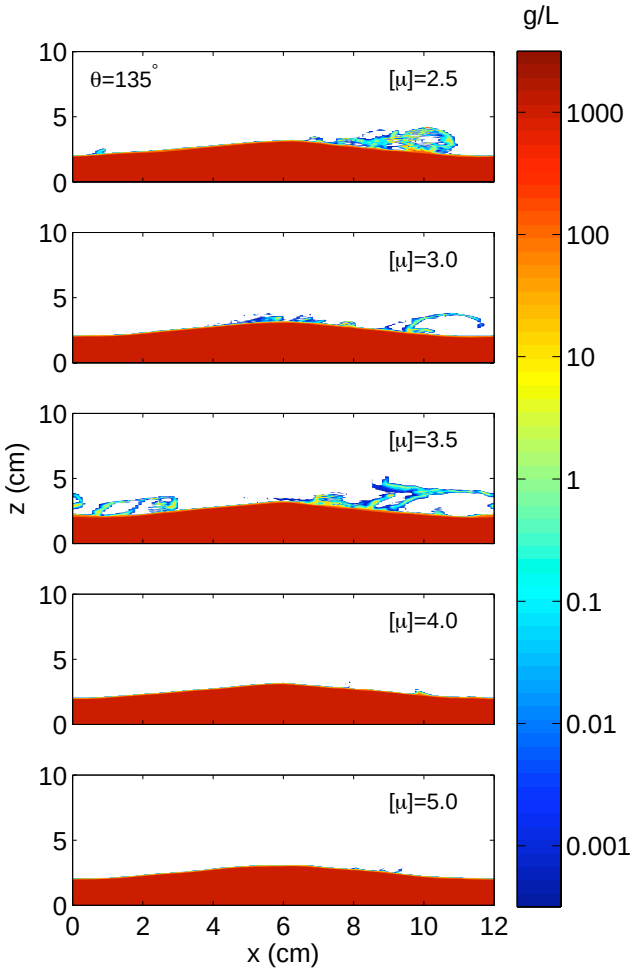

Fig. 5. Suspended sediment concentration fields ensemble averaged over three wave periods at maximum flow deceleration ($\theta = 135°$) for varying intrinsic viscosities.

At maximum flow acceleration (Figure 4), the suspended sediment spread throughout the domain but concentrated over the peak of the ripple. Again, the lower intrinsic viscosity simulations had greater amounts of suspended sediment in the water column than the higher intrinsic viscosity simulations. The turbulent vortices generated in the beginning of the phase advected to the right side of the ripple and began to settle out at maximum flow deceleration (Figure 5) for the lower intrinsic viscosity simulations. As the intrinsic viscosity increased from 2.5 to 3.5, the turbulent vortices stretched horizontally and one can observe a slight phase lag between the vortex centers. Almost all the suspended sediment had settled in the higher viscosity simulations.

A quantitative analysis of the amount of suspended sediment in the water column confirmed the qualitative comparison in Figures 3, 4, and 5. A time series of the sum of the total suspended sediment in the water column shows approximately a 16% difference between the lower intrinsic viscosity and higher intrinsic viscosity simulations (Figure 6). The amount of suspended sediment in the water column also varied more with the phase in the lower intrinsic viscosity than the higher intrinsic viscosity simulations. We also examined the time series of suspended sediment concentration over the crest of the ripple (x=6 cm) ensemble averaged over the last 3 periods for all five simulations (Figure 7). Sediment plumes over the ripple crest occurred at approximately the same phase of the flow and height in the water column for the lower intrinsic viscosity values. However, the large difference in the amount of suspended sediment over the ripple crest between the lower intrinsic viscosity and the higher viscosity simulations remained evident.

B. Effective Viscosity Formulations

Numerous effective viscosity equations are available for the sediment phase viscosity closure in mixture theory. We use a modified version of Eilers' equation [11] in SedMix3D because it is well documented as successfully numerically modeling the viscosity of suspension flows. The equation is advantageous for coastal sediment transport by allowing the particle shape to vary with the intrinsic viscosity parameter.

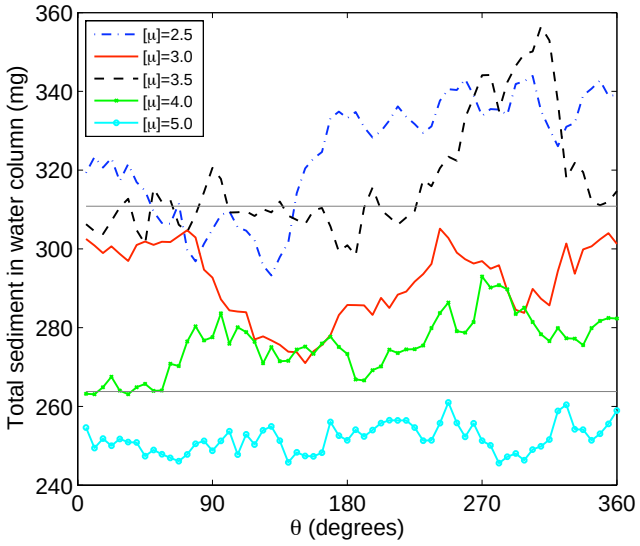

Fig. 6. Time series of total suspended sediment above the ripple profile ($\phi < 0.58$) ensemble averaged over three wave periods. Solid gray lines represent the phase averaged total suspended sediment amount for the lower intrinsic viscosity and higher intrinsic viscosity simulations, respectively.

Here, we examined the sensitivity of suspended sediment concentrations predicted by the model by replacing (4) with two additional common effective viscosity equations. The first effective viscosity equation will be referred to here as the Krieger-Dougherty equation (12) and is given as,

$$\frac{\mu}{\mu_f} = \left[1 - \frac{\phi}{\phi_m}\right]^{-\phi_m[\mu]}. \tag{12}$$

The second effective viscosity equation will be referred to here as the Mooney equation (13) and is given as,

$$\frac{\mu}{\mu_f} = \exp\left[\frac{[\mu]\phi}{1 - \phi/\phi_m}\right]. \tag{13}$$

Note that both (12) and (13) contain the same intrinsic viscosity, maximum packing concentration, and approximately equal maximum viscosities as our original effective viscosity formulation (4). The ϕ_m parameter for the Mooney equation was taken to be 0.82 to keep the maximum viscosity consistent between the simulations. Our baseline simulation here is the simulation described above using (4) with the intrinsic viscosity, $[\mu] = 3.0$. Both (12) and (13) were inserted into the model with an intrinsic viscosity, $[\mu] = 3.0$, and all other parameters including wave forcing conditions constrained as described above and in the Methodology. We compared the model output for the three different effective viscosity formulations. Figure 8 is a plot of the scaled effective viscosity versus volume fraction of sediment, ϕ, for the three effective viscosity formulations. All three equations result in similar effective viscosities for $0 < \phi < 0.4$. The Mooney equation (13) produces the highest viscosity of the three equations for $\phi > 0.4$ (Figure 8).

The concentration fields at flow reversal ($\theta = 0°$), and at maximum flow acceleration ($\theta = 45°$ and $\theta = 225°$) for the three effective viscosity equation simulations ensemble averaged over three wave periods are plotted in Figures 9, 10, and 11. A qualitative comparison of the simulations showed much less suspended sediment above the ripple in the Mooney simulation than the Eilers and Krieger-Dougherty simulations. At flow reversal (Figure 9), the turbulent vorticies were clearly defined and were at similar locations along the ripple and heights in the water column in the Eilers and Krieger-Dougherty simulations. There were no defined vortices in the Mooney simulation. At maximum flow acceleration (Figures 10 and 11), there

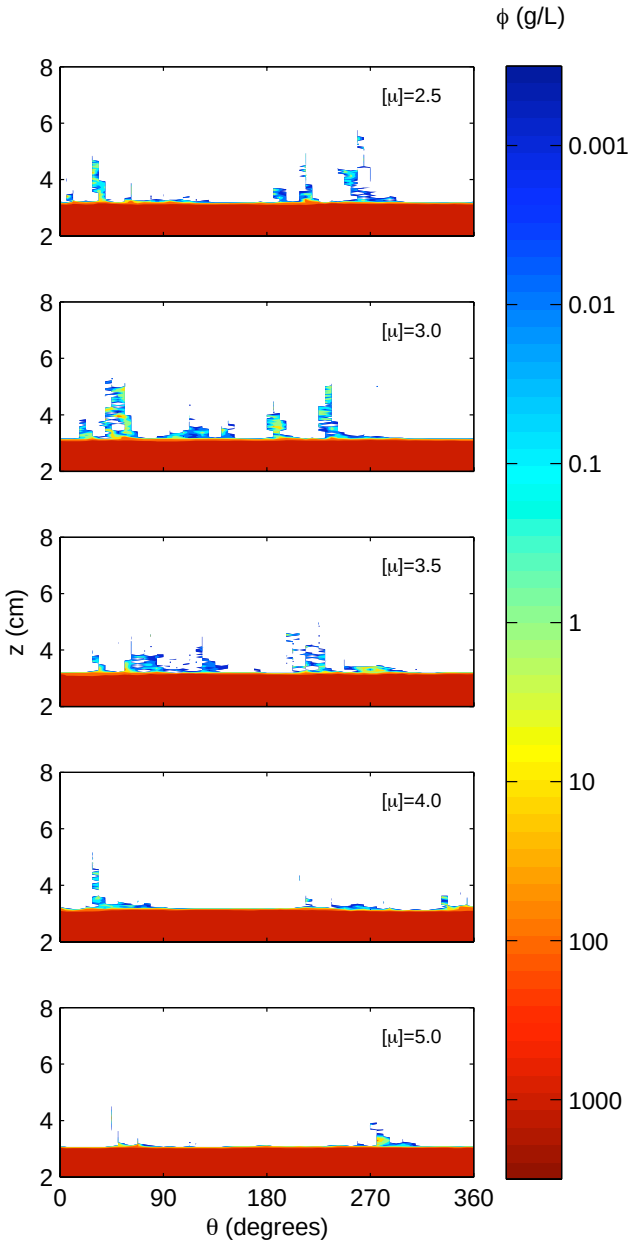

Fig. 7. Time series of the suspended sediment concentrations over the crest of the ripple ensemble averaged over three wave periods.

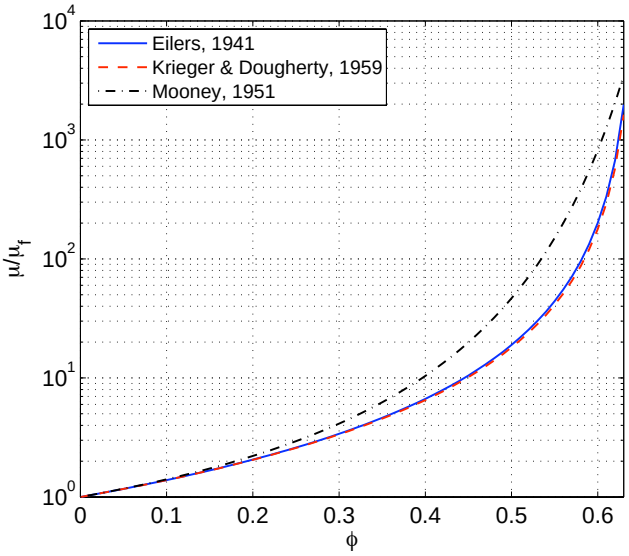

Fig. 8. Three scaled effective viscosity formulations, μ/μ_f versus volume fraction of sediment, ϕ.

was again much more suspended sediment in the Eilers and Krieger-Dougherty simulations than the Mooney simulation. The suspended sediment plume locations along the ripple profile and heights in the water column were almost identical in the Eilers and Krieger-Dougherty simulations. Figure 12 is a plot of the quantitative analysis of the suspended sediment above the ripple for the three simulations. There exists about a 14% difference between the average amount of total suspended sediment in the Krieger-Dougherty and Mooney simulations, but only about a 5% difference between the Krieger-Dougherty and Eilers simulations. The phase of maximum suspended sediment is not consistent between the simulations; however, the suspended sediment from the Eilers and Krieger-Dougherty simulations varies within a greater range throughout the flow phase than in the Mooney simulation. The amount of suspended sediment above the ripple crest (x=6 cm) throughout a wave period is plotted in Figure 13. The amount and height of the sediment was fairly consistent between the Eilers and Krieger-Dougherty simulations. The only phase at which there was a significant amount of suspended sediment above the ripple crest in the Mooney simulation was when the flow was accelerating from 0 to 40 cm/s.

IV. Discussion

A. Intrinsic Viscosity

At flow reversal, turbulent eddies shed off the left side of the ripple, picking up sediment into the water column. In all five of the simulations employing the Eilers equation (4) at 0° phase, the sediment is picked up on the left side of the ripple and advected by the turbulent eddies (Figure 3). However, for the three lower intrinsic viscosity simulations, the suspended sediment concentrations are much greater than the higher intrinsic viscosity simulations. Increasing the effective viscosity of the mixture causes a dampening of turbulent eddies and therefore, less suspended sediment. The decreased amount of turbulent eddies in the higher viscosity simulations is evident at all three phases shown (Figures 3-5). At maximum flow acceleration (Figure 4), turbulent eddies have broken up and spread the suspended sediment across the ripple profile. The suspended sediment is again in similar locations (over the entire crest of the ripple) and at similar heights in all the simulations. Increasing the intrinsic viscosity also affects the horizontal stretching of the turbulent eddies. At maximum deceleration, (Figure 5), the width of the eddies increase as $[\mu]$ increases from 2.5 to 3.5; however, the height of the eddies stays fairly constant.

A quantitative analysis of the total suspended sediment in the water column reveals that the lower intrinsic viscosity simulations have on average about 16% more sediment suspended than the higher intrinsic viscosity simulations. The viscosity of the mixture increases as the intrinsic viscosity value increases, and the sediment will advect less for larger intrinsic viscosities. Only an 11% difference in average suspended sediment exists between the lower intrinsic viscosity simulations. The

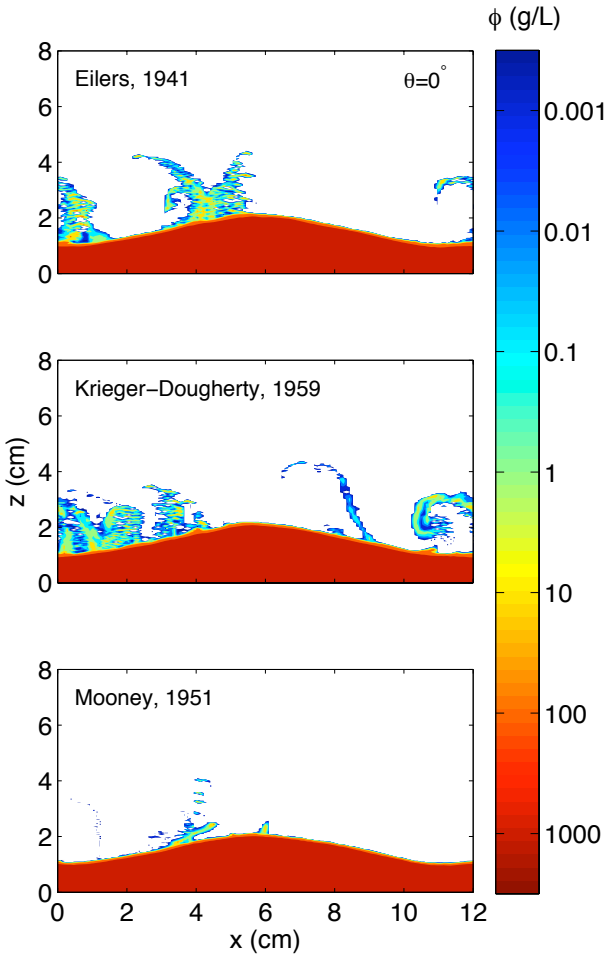

Fig. 9. Suspended sediment concentration fields ensemble averaged over three wave periods at flow reversal ($\theta = 0°$) for varying intrinsic viscosities.

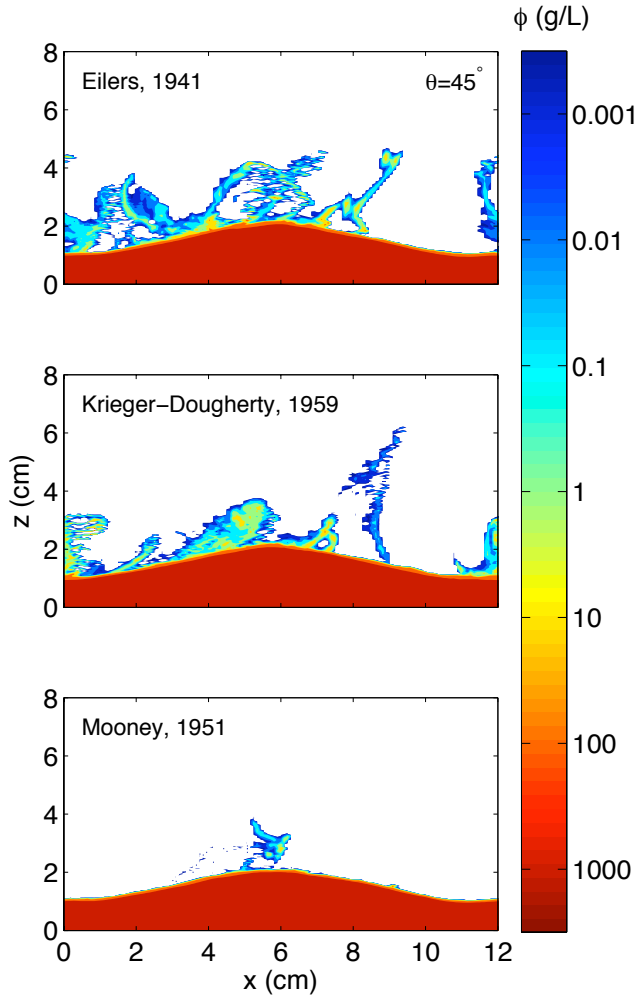

Fig. 10. Suspended sediment concentration fields ensemble averaged over three wave periods at flow reversal ($\theta = 45°$) for varying intrinsic viscosities.

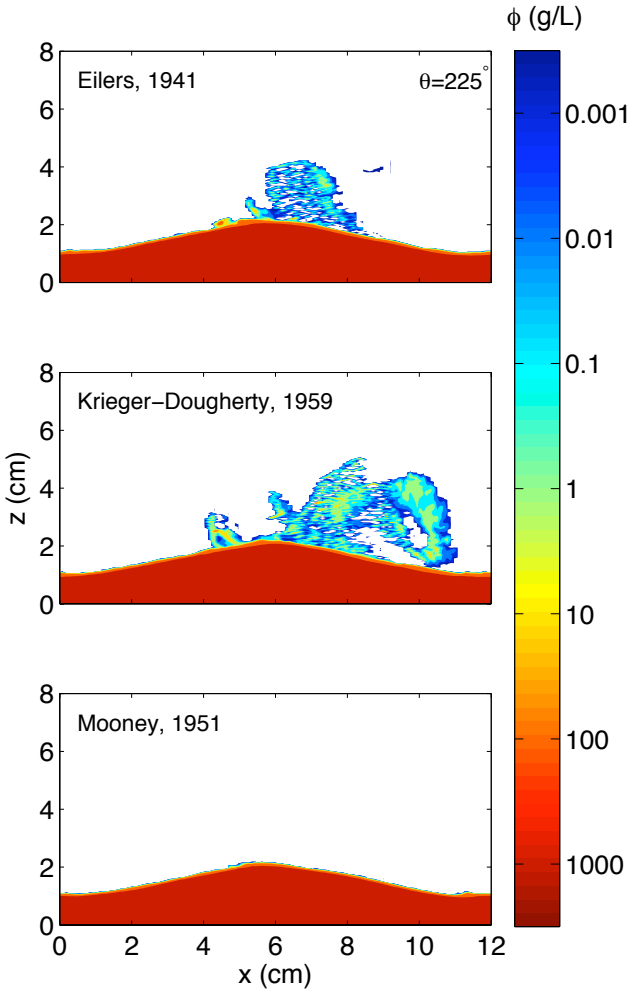

Fig. 11. Suspended sediment concentration fields ensemble averaged over three wave periods at flow reversal ($\theta = 225°$) for varying intrinsic viscosities.

most significant difference in the effective viscosity occurs at concentrations greater than 0.4 volume fraction (Figure 2). In a rippled bed environment, concentrations range from 0.4 to 0.6 at the ripple-fluid interface, where the differences between the effective viscosities are large. However, most of the suspended sediment occurs between $0.0 < \phi < 0.3$, where the difference in effective viscosity is not as prominent. Therefore, once the sediment gets picked up into the water column, the difference in the effective viscosity has less of an impact on the output. However, it is unknown why there is a 16% difference between lower intrinsic viscosity and the higher intrinsic viscosity simulations, but only about a 10% difference between the total suspended sediment concentration within the two groups. Intrinsic viscosity values in the higher range ($4 < [\mu] < 5$) correspond to a sediment axis ratio of about 5, which is significantly larger than the typical values of quartz sand (1-3). The range between the maximum and minimum amount of suspended sediment is also greater in the lower viscosity simulations than the higher viscosity simulations. The amount of sediment in suspension varies with the flow phase in the lower intrinsic viscosity simulations, which is consistent with laboratory and field observations. We use an intrinsic viscosity value of 3.0 for the numerical simulations of sediment transport because it produced the median amount of suspended sediment within the five simulations. Simulations using the 3.0 value predicted small-scale bedform heights and lengths that are in good agreement with common ripple predictor methods and shapes similar to those found in the laboratory and field [26]. Simulated concentration fields, specifically the location and phasing of sediment plumes, were found qualitatively consistent with laboratory measurements.

B. Effective Viscosity Formulations

By choosing three different common effective viscosity formulations, we tested the sensitivity of SedMix3D to the sediment phase effective viscosity closure. Of the three effective viscosity formulations we tested, the widely accepted Eilers and Krieger-Dougherty equations had very similar output. However, the Mooney equation generated much less suspended sediment in the water column than the other two formulations.

The Krieger-Dougherty equation produced the most suspended sediment on average, about 14% more than the Mooney equation and about 5% more than the Eilers equation (Figure 12). The suspended sediment predicted in the Krieger-Dougherty and Eilers simulations also varies more with the flow phase than the suspended sediment in the Mooney simulation, which suggests that decreasing the effective viscosity will increase the response of the sediment to the flow.

The effective viscosities produced from the formulations increasingly differ as $\phi > 0.4$ (Figure 8), which is approximately the concentration of the region at the interface between the ripple and fluid. In this region, the sediment grains are rolling and sliding over the packed bed, are picked up, and are advected into the water column. As the effective viscosity increases in this region, less grains will be picked up by the flow, decreasing the amount of suspended sediment. The model seems to be sensitive to differences in effective viscosity at concentrations between about 0.4 and 0.6 volume fraction. As the intrinsic viscosity simulations showed, once the sediment is advected into the water column, the difference in the effective viscosity does not significantly affect the concentration field output from the simulations.

C. Model Limitations

Mixture theory subsumes the physics of fluid-sediment interactions in the bottom boundary layer to numerically model coastal sediment transport. However, due to the high resolution of the grid, the model is very computationally expensive (about 75 days of CPU time for a 10 s three-dimensional simulation). Here, the simulations are quasi-three-dimensional to approximate the model's three-dimensional behavior in a more reasonable amount of time (about one week per simulation). A quasi-three-dimensional simulation has full dimensions in the x- and z-directions, but has only two grid points in the y-direction. The concentration is then summed over the two grid points in the y-direction to obtain a concentration field in the x- and z-domain. The reduction of grid points ultimately reduces the computational time by a factor of about 10; however, we found a significant difference between the effects of three-dimensional vortex structures and two-dimensional structures on the turbulent flow and sediment transport. Parallel algorithms are being developed to allow for three-dimensional simulation domains to approach laboratory scales.

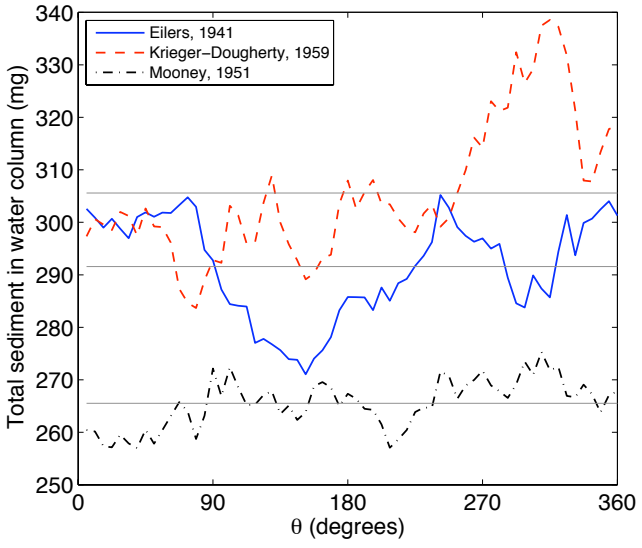

Fig. 12. Time series of total suspended sediment above the ripple profile ($\phi < 0.58$) ensemble averaged over three wave periods. Solid gray lines represent the phase averaged total suspended sediment amount for the Krieger-Dougherty, Eilers, and Mooney formulation simulations, respectively.

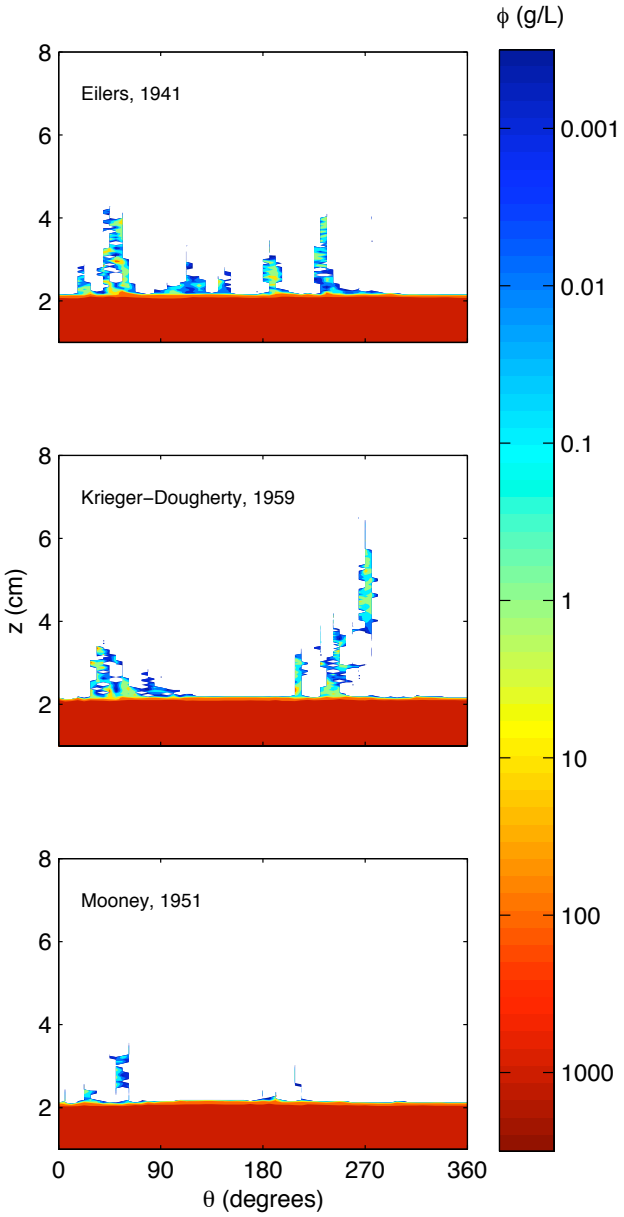

Fig. 13. Time series of the suspended sediment over the crest of the ripple ensemble averaged over three wave periods.

V. Conclusions

Although mixture theory has been well documented as an effective approach to numerically model suspension flows, it has not yet been applied to study sediment transport over rippled sand beds. Here, we tested the model sensitivity to the effective viscosity by varying an adjustable parameter within the effective viscosity formulation in SedMix3D. By varying the intrinsic viscosity value between 2.5 and 5.0, we found the lower values ($[\mu] = 2.5$, 3.0, and 3.5) generate on average about 16% more suspended sediment in the water column than the higher intrinsic viscosity values ($[\mu] = 4.0$ and 5.0). However, within the two groups, the total suspended sediment in the water column varied by approximately 10%. The locations of the sediment plumes were similar within the two groups of simulations; however, the suspended sediment plume concentrations in the higher intrinsic viscosity simulations were less than the lower intrinsic viscosity simulations. Therefore, choosing an intrinsic viscosity value within the range of 2.5-3.5 when employing Eilers' equation will not significantly affect the model output for the presented simulation conditions.

Additionally, we tested the model sensitivity to two other effective viscosity formulations while keeping the intrinsic viscosity and forcing conditions constant. There is a slight difference in the model output between the Eilers and Krieger-Dougherty effective viscosity formulations; however, a large difference exists between the output from the Mooney effective viscosity equation and the other two equations. The difference suggests a higher model sensitivity to variations in the effective viscosity within the ripple-fluid interface ($0.4 < \phi < 0.6$) than the suspended sediment concentration range ($0.0 < \phi < 0.3$). The variations in the total suspended sediment with the flow phase in each simulation suggests that the suspended sediment's response to the flow increases with decreasing effective viscosity. Comparisons of concentration fields to laboratory data should provide insight to the most accurate effective viscosity equation and intrinsic viscosity value for specific sediment sizes and distributions; however, using either Eilers' or Krieger-Dougherty's equation with an intrinsic viscosity, $[\mu] = 3.0$, did not significantly affect the simulation predictions of suspended sediment concentration for the range of conditions tested here.

Acknowledgments

AMP and JC are supported under base funding to the Naval Research Laboratory from the Office of Naval Research (PE#61153N). Partial support for AMP is also provided by the Office of Naval Research Code 322 Coastal Geosciences Program. This work was supported in part by a grant of computer time from the DoD High Performance Computing Modernization Program at the NAVY DSRC and the ERDC DSRC.

References

[1] P. Scandura, G. Vittori, and P. Blondeaux, "Three-dimensional oscillatory flow over steep ripples," *Journal of Fluid Mechanics*, vol. 412, pp. 355–378, 2000.

[2] B. C. Barr, D. N. Slinn, T. Pierro, and K. B. Winters, "Numerical simulation of turbulent, oscillatory flow over sand ripples," *Journal of Geophysical Research*, vol. 109, no. C9, pp. 1–19, 2004.

[3] Y. S. Chang and A. Scotti, "Turbulent convection of suspended sediments due to flow reversal," *Journal of Geophysical Research*, vol. 111, no. C7, p. C07001, 2006.

[4] A. Nir and A. Acrivos, "Sedimentation and sediment flow on inclined surfaces," *Journal of Fluid Mechanics*, vol. 212, pp. 139–153, 1990.

[5] P. Nott and J. Brady, "Pressure-driven flow of suspensions - simulation and theory," *Journal Of Fluid Mechanics*, vol. 275, pp. 157–199, SEP 25 1994.

[6] I. Miskin, L. Elliott, D. B. Ingham, and P. S. Hammond, "The viscous resuspension of particles in an inclined rectangular fracture," *International Journal Of Multiphase Flow*, vol. 22, no. 2, pp. 403–415, 1996.

[7] ——, "Steady suspension flows into two-dimensional horizontal and inclined channels," *International Journal Of Multiphase Flow*, vol. 22, no. 6, pp. 1223–1246, 1996.

[8] M. Hofer and K. Perktold, "Computer simulation of concentrated fluid-particle suspension flows in axisymmetric geometries," *Biorheology*, vol. 34, no. 4-5, pp. 261–279, Jul. 1997.

[9] D. W. Sun, S. R. Annapragada, and S. V. Garimella, "Experimental and numerical study of melting of particle-laden materials in a cylinder," *International Journal Of Heat And Mass Transfer*, vol. 52, no. 13-14, pp. 2966–2978, Jun. 2009.

[10] A. Einstein, "Eine neue Bestimmung der Moleküldimensionen (German) [A new determination of molecular dimensions]," *Annalen der Physik*, vol. 19, pp. 289–306, 1906.

[11] H. Eilers, "The viscosity of the emulsion of highly viscous substances as function of concentration," *Kolloid-Zeitschrift*, vol. 97, no. 3, pp. 313–321, 1941.

[12] M. Mooney, "The viscosity of a concentrated suspension of spherical particles," *Journal of Colloid Science*, vol. 6, no. 2, pp. 162–170, 1951.

[13] I. M. Krieger and T. J. Dougherty, "A mechanism for non-newtonian flow in suspensions of rigid spheres," *Journal of Rheology*, vol. 3, no. 1, pp. 137–152, 1959.

[14] I. M. Krieger, "Rheology of monodisperse latices," *Advances in Colloid and Interface Science*, vol. 3, no. 2, pp. 111 – 136, 1972.

[15] F. Ferrini, D. Ercolani, B. D. Cindio, L. Nicodemo, L. Nicolais, and S. Ranaudo, "Shear viscosity of settling suspensions," *Rheologica Acta*, vol. 18, no. 2, pp. 289–296, 1979.

[16] D. Leighton and A. Acrivos, "The shear-induced migration of particles in concentrated suspensions," *Journal of Fluid Mechanics*, vol. 181, pp. 415–439, 1987b.

[17] B. de Cindio, L. Nicodemo, and P. Masi, "On the non-newtonian behavior of suspensions," *Rheologica Acta*, vol. 26, no. 1, pp. 100–101, 1987.

[18] R. D. Sudduth, "A generalized-model to predict the viscosity of solutions with suspended particles .1." *Journal Of Applied Polymer Science*, vol. 48, no. 1, pp. 25–36, Apr. 1993.

[19] M. Hunt, R. Zenit, C. Campbell, and C. Brennen, "Revisiting the 1954 suspension experiments of R. A. Bagnold," *Journal of Fluid Mechanics*, vol. 452, pp. 1–24, 2002.

[20] V. Vand, "Viscosity of solutions and suspensions .1. theory," *Journal of Physical and Colloid Chemistry*, vol. 52, no. 2, pp. 277–299, 1948.

[21] N. Huang and D. Bonn, "Viscosity of a dense suspension in couette flow," *Journal Of Fluid Mechanics*, vol. 590, pp. 497–507, Nov. 2007.

[22] M. A. Nawab and S. G. Mason, "The viscosity of dilute suspensions of thread-like particles," *Journal Of Physical Chemistry*, vol. 62, no. 10, pp. 1248–1253, 1958.

[23] R. A. Bagnold, "Experiments on a gravity-free dispersion of large solid spheres in a Newtonian fluid under shear," *Proceedings of the Royal Society of London, Series A*, vol. 225, no. 1160, pp. 49–63, 1954.

[24] J. F. Richardson and W. N. Zaki, "Sedimentation and fluidisation: part 1," *Transactions of the Institution of Chemical Engineers*, vol. 32, pp. 35–53, 1954.

[25] D. Leighton and A. Acrivos, "Viscous resuspension," *Chemical Engineering Science*, vol. 41, no. 6, pp. 1377–1384, 1986.

[26] A. M. Penko, "Modeling sand ripple evolution under wave boundary layers," Master's thesis, University of Florida, 2007.